J Mater Sci (2025) 60:11517–11528

Comparative study of microstructural influence on corrosion resistance in conventional and Al-Mn quasicrystalline cast aluminum alloys

Mirjam Bajt Leban[1,*], Tim Drevenšek[2], Tadeja Kosec[1], Blaž Leskovar[2], and Boštjan Markoli[2]

[1] *Slovenian National Building and Civil Engineering Institute, Dimičeva 12, 1000 Ljubljana, Slovenia*
[2] *Department of Materials and Metallurgy, Faculty of Natural Sciences and Engineering, University of Ljubljana, Aškerčeva cesta 12, 1000 Ljubljana, Slovenia*

Received: 13 February 2025
Accepted: 23 May 2025
Published online: 30 June 2025

ABSTRACT

The investigation focused on the quasicrystalline aluminum alloy Al-Mn-Cu-Mg-Si-Ti. The influence of microstructure of aluminum alloy strengthened with quasicrystals on its corrosion resistance was studied. The properties of newly designed quasicrystalline aluminum alloy (QC) were compared to the properties of standard AlSi9Cu3 alloy (DIN 226). Both aluminum alloys (QC and AlSi9Cu3) were cast in a steel die with a controlled cooling rate. After the preparation of the samples, the microstructural characterization was carried out. In the quasicrystalline alloy, the microstructure was dominated by a primary phase with fivefold symmetry, representing the quasicrystalline phase. To investigate corrosion properties, open-circuit potential, linear polarization and potentiodynamic polarization measurements were performed. The influence of corrosion on mechanical properties was studied by conducting tensile tests on environmentally exposed alloys. It was concluded that the quasicrystalline alloy has comparable corrosion properties to the commercially widely used AlSi9Cu3 alloy. In the latter alloy, corrosion was observed to initiate in the vicinity of the Al_2Cu intermetallic compound particles. In the case of the QC alloy, corrosion attacked mainly the α_{Al} phase (matrix).

Handling Editor: Nima Haghdadi.

Address correspondence to E-mail: mirjam.bajt-leban@zag.si

https://doi.org/10.1007/s10853-025-11046-7

GRAPHICAL ABSTRACT

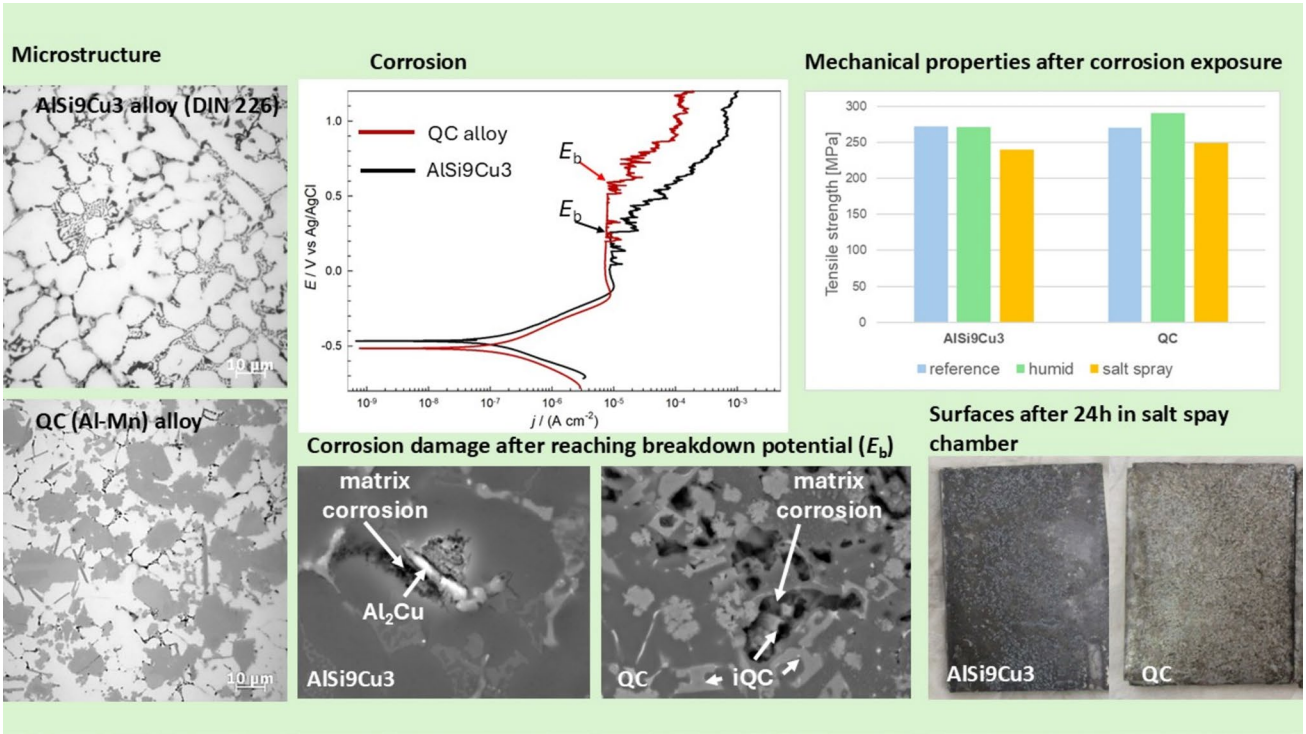

Introduction

Aluminum alloys play a crucial role in numerous industries, including aerospace [1, 2], automotive [3, 4], construction [5, 6] and packaging [7], due to their lightweight, versatility and desirable properties. Their low density, which contributes to reduced product weight, combined with favorable mechanical characteristics and strong corrosion resistance, positions them as important materials in advanced technologies [8].

Quasicrystals in Al-Mn alloy were observed for the first time in 1984 [9, 10]. Further studies revealed their high hardness, low friction and good wear resistance [11]. This aluminum alloy development is significant for global sustainability efforts, as it supports the goals of reducing carbon emissions and promoting the use of sustainable materials due to its high recyclability [12]. Its enhanced mechanical properties enable reduced material usage and lower component weight, contributing to improved fuel efficiency in transportation. Additionally, the incorporation of quasicrystals enables resource efficiency by reducing the reliance on silicon (Si), further contributing to more sustainable use of natural resources, as found by the life cycle assessment (LCA) analysis of the EIT Raw Materials project CastQC.

The corrosion resistance of metallic materials is a critical determinant of their long-term performance and reliability in diverse applications, directly influencing their structural integrity, durability and overall functionality in challenging environments. Aluminum alloys exhibit excellent corrosion resistance due to the formation of a protective oxide layer. However, the degree of resistance can fluctuate depending on the specific alloy composition, microstructure and environmental factors [13]. The influence of alloying elements in solid solution affects measured open-circuit potential (E_{OCP}) [13]. Among alloying elements, only Mg and Zn have a good solubility in aluminum [13]. The solubility of other chemical elements is lower and therefore during solidification, intermetallic compounds are formed. The presence of intermetallic phases, which are enriched with various alloying elements, can initiate localized instead uniform corrosion [13]. The corrosion resistance of aluminum alloy depends on the chemical composition of intermetallics and their distribution. Electrochemical potential of intermetallics in relation to aluminum matrix can be either cathodic or anodic. In the case of the cathodic

intermetallic phase, its corrosion potential (E_{corr}) is higher than that of the matrix which causes corrosion of the latter. When the E_{corr} of intermetallic phase is lower, aluminum matrix will remain intact, while anodic phase will corrode [14, 15]. Copper is added as an alloying element to aluminum to enhance its strength through the formation of various intermetallic compounds. Among the Al-Cu intermetallics tested in NaCl aqueous solutions of varying concentrations, Al_2CuMg exhibited the lowest corrosion potential (E_{corr}). The differences in Ecorr between Al_7Cu_2Fe, Al_2Cu and $Al_{20}Cu_2Mn_3$ were minor; however, their E_{corr} values decreased as the NaCl concentration in the testing environment increased [15]. For example, Al_2CuMg phase is anodic, while Al_2Cu phase is cathodic in respect to the matrix [16]. Anodic Al_2CuMg phase is dealloyed, which causes Cu deposition around intermetallics and preferential corrosion of aluminum matrix because of galvanic effect [15, 17]. While the influence of Cu on the corrosion of aluminum alloys is well studied, the Mn is generally considered a less harmful alloying element in terms of corrosion [15, 18–20]. Based on the available literature mentioned previously, it can be concluded that Mn-based intermetallics in aluminum alloys are in general cathodic.

Al-Mn quasicrystals are in nature different from Al-Mn intermetallics in their structure which is not crystalline but quasicrystalline, i.e., exhibiting quasi-periodicity. This in turn is also strongly related to the different corrosion behavior of quasicrystalline phases vs. their intermetallic counterparts as the nature of the atomic bond is closer to the metallic bond. Their chemical and structural compositions differ significantly and influence corrosion properties. The influence of Al-Mn quasicrystals on the corrosion behavior of aluminum alloys was barely studied [21] in the past. The aim of the present study was to compare corrosion resistance using electrochemical methods and determination of mechanical properties after environmental exposures. To bridge the gap between the understanding of corrosion behavior and microstructural characteristics, the surface after electrochemical potentiodynamic polarization was carefully examined by using a scanning electron microscope and spectroscopy.

Materials and methods

Standardized DIN 226 alloy (AlSi9Cu3, EN AB 4600), and a novel quasicrystalline, QC alloy (Al-Mn-Cu-Mg-Si-Ti), were cast in the laboratory. To prepare both alloys, in the first step, the 99.9% pure aluminum was added to the graphite crucible and melted at the furnace preheated to 880 °C. During the stirring of the melt, alloying elements were added. After the complete melting of all constituents, the melt was cast into the steel mold, which was preheated to 250 °C, and afterward cooled in water. The chemical composition of both cast alloys, defined by optical emission spectroscopy method (SpectroMAXx, Spectro, Germany) is presented in Table 1.

After casting, specimens were machined by milling to desired geometries for metallographic and corrosion tests. At least 1-mm-thick surface layer was removed from cast parts. Metallographic samples were ground to 320 SiC, followed by polishing sequentially with 9 μm, 3 μm and 1 μm diamond suspensions (MetaDi Supreme Polycrystalline Suspension) with the addition of water-soluble extender (MetaDi Fluid), and finished with amorphous colloidal silica (0.06 μm). Microstructure was observed by optical microscope (Axio Imager Z2, Carl Zeiss) on as polished specimens. X-ray diffraction (XRD) analysis was carried out using an Empyrean XRD diffractometer (PANalytical, Malvern, UK) and the data were analyzed using HighScore Plus database software. The XRD spectra were measured between 4° and 100° (2Θ), using a step size of 0.0065° and a time per step of 61.2 ms.

Before electrochemical testing, all samples were ground to 600 SiC, rinsed with deionized water and ethanol and air-dried. A three-electrode corrosion cell was used for electrochemical tests, consisting of a working electrode (a cylindrical flat specimen of diameter 15.0 mm, inserted in the specimen holder, so that an effective area of 0.785 cm^2 was exposed to the solution), a reference electrode (Ag/AgCl/KCl (sat.)), and a graphite rod as a counter electrode. As an electrolyte phosphate buffer solution pH 7 with 1 mM NaCl, phosphate buffer was prepared by combining 1L of 0.68% KH_2PO_4 and 291 mL 0.1 M NaOH. The open-circuit potential

Table 1 Chemical composition of cast AlSi9Cu3 and QC alloy, all results are in weight %

Alloy	Al	Mn	Si	Cu	Mg	Fe	Ti	Zn
AlSi9Cu3	85.8	0.27	9.43	2.27	0.31	0.76	0.05	0.88
QC	89.4	5.76	0.42	3.37	0.57	0.11	0.40	0.01

(OCP) was measured for 1 h, followed by polarization resistance measurement (LP) in the range of ± 20 mV around OCP with scanning rate of 0.1 mV/s. After that electrochemical impedance measurements (EIS) were conducted in the frequency range from 65 kHz to 1 mHz with an AC amplitude of ± 10 mV. As a last electrochemical measurement, potentiodynamic polarization (PD) was conducted by increasing potential with scan rate 1 mV/s from − 0.25 V versus OCP increasing in the anodic direction. The surfaces of specimens intended for further microscopic examination after the PD test were polished with 0.06 µm amorphous colloidal silica. The experiment on these specimens was terminated when the current density reached 0.1 mA/cm^2 to enable damage comparison. Surface examination was carried out using a scanning electron microscope (SEM, JEOL JSM IT500LV) coupled with an energy x-ray dispersive spectroscopy (EDS, AZtec ADV XMAX 65 EDX detector and AZtec 4.3 software).

To investigate corrosion influence on mechanical properties, the tensile tests were conducted following the SIST EN ISO 6892-1:2017 standard, Method B using tensile testing machine Zwick/Roell Z30 with a 3-kN force cell. Tests were conducted on flat standard specimens which were previously not exposed to a corrosion environment and those that were exposed for 10 cycles to a humid atmosphere (one cycle consists of 8 h in the humid chamber at 40 °C according to EN ISO 6270-1 and 16 h at the air), or for 10 cycles in the salt atmosphere (one cycle consists of 8 h in salt spray chamber 35 °C according to SIST EN ISO 9227 NSS: 2023 and 16 h in the air).

Results and discussion

Microstructure

Figure 1 depicts the characteristic microstructure of AlSi9Cu3 alloy, consisting of the matrix (white), α_{Al} phase, with a dendritic morphology. The areas appearing between the dendrites are mainly eutectic ($\alpha_{Al} + \beta_{Si}$). Since the alloy is hypoeutectic (contain less than 12.6 wt% Si), a "mesh"-like structure of the secondary phase appears in between dendrites of the primary α_{Al}. In the microstructure also intermetallic Mg_2Si, Al_2Cu and Al_2CuMg phases, enriched with Cu, are present in small amounts. The amount of Cu-rich phases in this alloy, as measured by ImageJ software, was approximately 1.8%. It is noteworthy that all

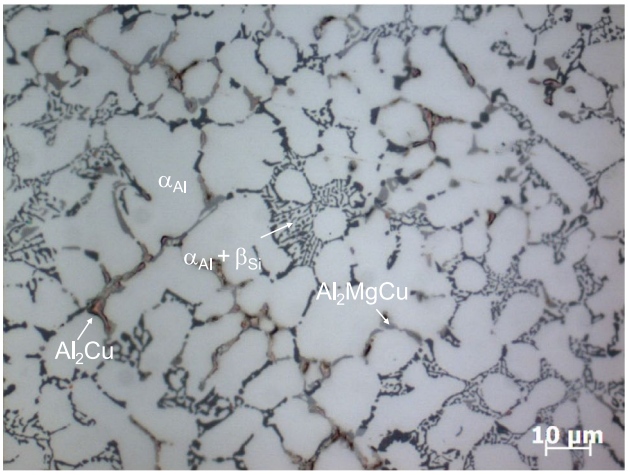

Figure 1 Light optical microcopy (LOM) image of microstructure of AlSi9Cu3 alloy with dominating, gray-colored binary eutectic ($\alpha_{Al}+\beta_{Si}$) and sporadic areas of brown-reddish-like areas containing other intermetallic phases containing copper, magnesium and silicon

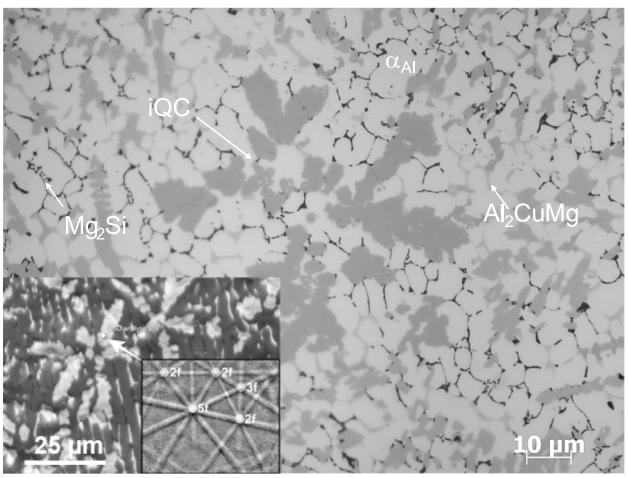

Figure 2 LOM image of microstructure of QC alloy with dendrites of α_{Al} matrix as dominant phase and large amount of bulky dark-gray iQC phase as second dominant phase, accompanied with small amounts of needle-like quasicrystalline approximant, denoted as α-AlMnSi phase; in the insert SEM image along with EBSD for iQC phase with five-, three- and twofold axes

intermetallic phases are integral parts of either binary, ternary or quaternary heterogeneous structures.

QC alloy microstructure, presented in Fig. 2, consists of the matrix (white), α_{Al}. On α_{Al} matrix grain borders, segregation of intermetallic Al_2Cu and Al_2MgCu phases can be seen [22, 23]. Quasicrystalline phase of gray color, enriched in Mn, is present randomly over the whole investigated surface. The amount of this

phase, as measured by ImageJ software on microstructure photograph taken at magnification of 200 ×, is around 26% in respect to the total observed surface, and the amount of Cu-rich phases is approximately 1.4%.

From XRD diffractogram in Fig. 3 for both alloys, it is clear and is consistent with the micrographs of the microstructure in Figs. 1 and 2, that matrix α_{Al} is dominant (Crystallography Open Database ID-COD ID 9008460). Other phases in the case of AlSi9Cu3 alloy of the diffractogram in Fig. 3, such as Al_2Cu (COD ID 9012196) and α-AlFeMnSi (ICDD database PDF#06-0669, [24]), exhibit only very small number of low-intensity peaks which can be related to the intermetallic phases typical for this alloy. In the case of QC alloy, additional peaks can be seen between the dominant one for the α_{Al} matrix, i.e., (111) and (200). These peaks are related predominantly with the presence of the iQC phase (ICDD database PDF-00-040-1233) and to those of the quasicrystalline approximant α-AlMnSi phase (COD ID 2007194) [21, 25]. Other phases, such as Al_6Mn (Materials Project (mp-173)), approximant α-AlMnSi (COD ID 2007194), Al_2CuMg (COD ID 7222567) and Mg_2Si (COD ID 1537740), also add to the complexity of the XRD diffractogram. The intensities for individual peaks may differ from those found in the database such as JCPDS because the microstructure is heavily textured because of semidirectional solidification. As analyzed by EDS, QC alloy quasicrystals contain 74.2 ± 1.6 wt% Al, 2.2 ± 0.5 wt% Cu, 21.6 ± 1.9 wt% Mn and 1.5 ± 0.2 wt% Ti.

Electrochemical properties

During the first hour of immersion into the environment, the shift to more positive potential was observed for both aluminum alloys (Fig. 4a). The open-circuit potential (E_{OCP}) value of AlSi9Cu3 is higher during the

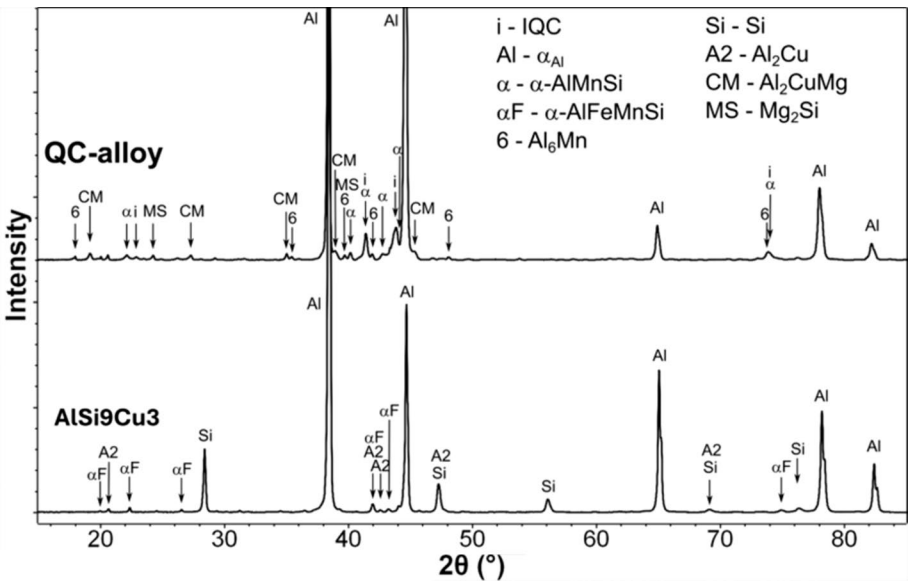

Figure 3 XRD patterns of the AlSi9Cu3 and QC alloy with peaks for the dominant phases in both alloys

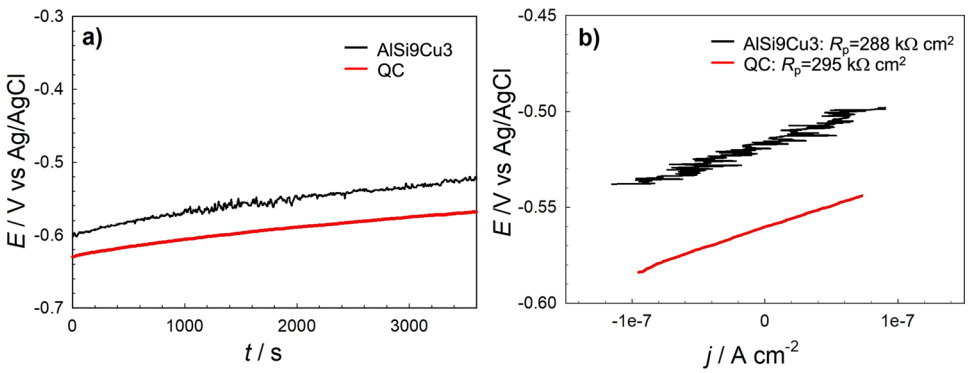

Figure 4 Open-circuit potential measurements (**a**) and linear polarization measurements (LP) (**b**) for the AlSi9Cu3 and QC alloy in not aerated phosphate buffer pH 7 with 1 mM NaCl, scan rate 1 mV/s

Table 2 Parameters obtained from the electrochemical measurements

		AlSi9Cu3	QC alloy
OCP	E_{OCP}(V)	−0.544 ± 0.023	−0.571 ± 0.037
LP	R_p (kΩ cm^2)	465 ± 155	469 ± 230
EIS	|Z| (kΩ cm^2)	290 ± 66	248 ± 16
PD	j_{corr} (μA/cm^2)	0.146 ± 0.028	0.145 ± 0.018
	j_{pass} (μA/cm^2)	8.491 ± 0.371	6.301 ± 0.758
	E_{corr} (V)	−0.499 ± 0.023	−0.524 ± 0.030

whole duration of this test. At the end of exposure (see also results in Table 2), the potential of alloy AlSi9Cu3 is more positive than that of QC alloy. However, the curve for AlSi9Cu3 is unstable and discontinued, with several sudden fluctuations in measured E_{OCP} value. Similar findings were reported by Zhang et al. [26] and Kakinuma et al. [27] for aluminium alloys exposed to a chloride test environment in which metastable pitting was observed.

Linear polarization measurements were conducted after reaching a steady state and are for the representative measurements presented in Fig. 4b. In the case of these measurements, R_p for AlSi9Cu3 was 288 kΩ cm^2 and for QC was 295 kΩ cm^2. The current fluctuations were observed in the case of AlSi9Cu3 alloy, showing micro-instabilities. This is also reflected in relatively low repeatability of measurements in the case of AlSi9Cu3 alloy; however, the scatter of results was also high in the case of QC alloy (see Table 2).

Potentiodynamic polarization curves for both aluminum alloys are presented in Fig. 5. Both cathodic and anodic behaviors up to − 0.2 V are similar for both alloys. However, by increasing potential in the anodic region, passive behavior is observed from constant current density on both alloys. The current fluctuations are observed for AlSi9Cu3 and at potential of around 0.26 V, the passive layer breaks down at breakdown potential E_b, denoted by black arrow in Fig. 5. Passive current density in the passive region for QC alloy is lower than for AlSi9Cu3. Some current fluctuations are observed for OC alloy, the width of passive range is higher, and E_b is also at more positive potentials at 0.60 V (denoted by red arrow in Fig. 5). Lower current densities in passive region, more positive breakdown potential E_b and fewer current fluctuations point at more favorable corrosion properties of QC alloy when compared to those of alloy AlSi9Cu3 under the given conditions.

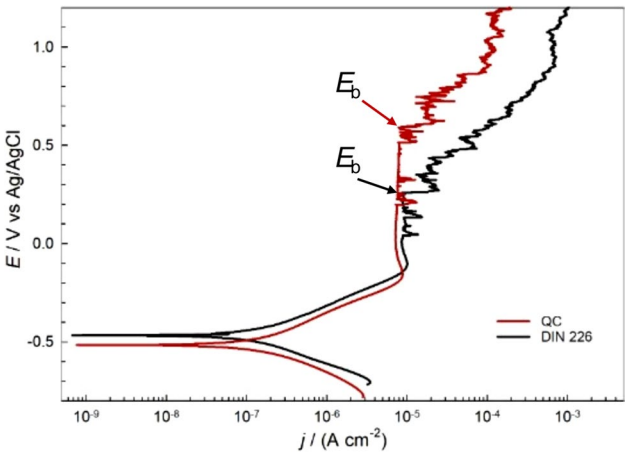

Figure 5 Potentiodynamic (PD) polarization curves for the AlSi9Cu3 and QC alloy in not dearated phosphate buffer pH 7 with 1 mM NaCl, scan rate 1 mV/s

Electrochemical impedance spectroscopy measurements were conducted at open-circuit potential. Figure 6 displays a representative EIS measurement for both alloys. As it can be seen from this Figure, impedance spectra for both alloys are similar. The fitted values in spectra are represented by a black line, which shows the curves fitted to the equivalent circuit (its scheme is plotted in the Nyquist plot in Fig. 6). In this circuit, Rs represents the solution resistance (66 Ω), Cdl represents the double layer capacitance, and R_p represents the polarization resistance of the oxide film on the aluminum alloy. The polarization resistance is 254 kΩcm^2 for the AlSi9Cu3 alloy and 243 kΩcm^2 for the QC alloy [28].

The results obtained from several repeated electrochemical measurements are shown as mean values with standard deviation in Table 2. In the appendix, in Supplementary figure S1, a scatter diagram is presented for all polarization resistance measurements for both alloys, where the surface for electrochemical measurements was prepared by conventional method, grinding and polishing. Outliers were presented in red dot and were not used for the standard deviation presentation of results in Table 2. The results from the electrochemical measurements presented in Table 2 indicate that the protective properties of both alloys are comparable. This conclusion is based particularly on the polarization resistance (R_p), which is calculated from linear polarization (LP) plots, and the absolute impedance (|Z|), which is obtained from the real part of the impedance at

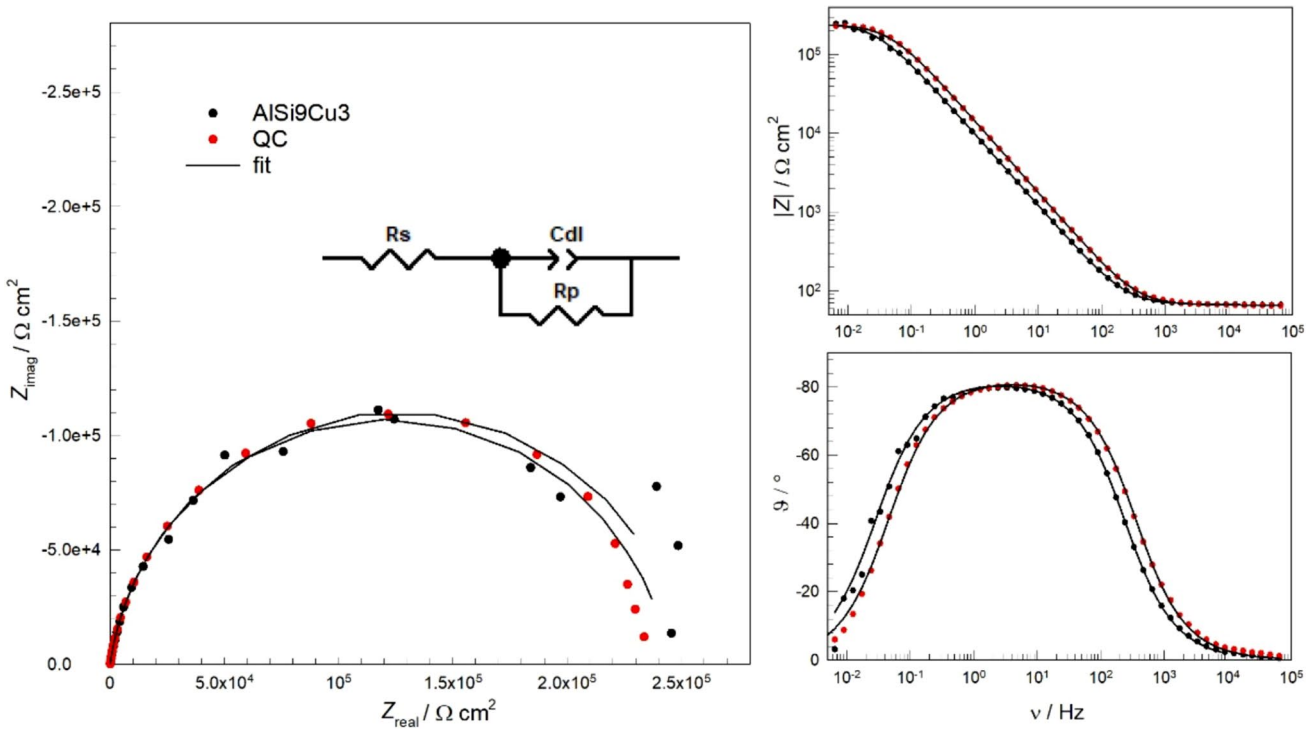

Figure 6 Electrochemical impedance spectroscopy (EIS) measurements, Nyquist and Bode plots, for the AlSi9Cu3 and QC alloy in phosphate buffer pH 7 with 1 mM NaCl

the lowest frequency. However, it should be noted that a significant degree of variability is exhibited in the linear polarization measurements, indicating instability in the oxide film.

Surface investigation after potentiodynamic polarization

During the potentiodynamic polarization at anodic potential, the breakdown of the passive layer on both alloys occurred. The potentiodynamic polarization was stopped when a current density of 0.1 mA/cm^2 was reached, so that the corrosion damage on the specimen surface was minimal.

In Fig. 7, a characteristic corrosion damage for AlSi9Cu3 alloy can be observed. Corrosion attack is located next to Al_2Cu intermetallic inclusion. This means that in this case, Al_2Cu acted cathodically, whereas a α_{Al} matrix behaved anodically, which is why it dissolved during anodic polarization. Similar observations where Al_2Cu behaved as a cathodic intermetallic phase were reported previously [29, 30]. It is known, that in an acidic environment, the corrosion potential of Al_2Cu (θ-phase) is several hundred millivolts higher than pure Al [15, 31]. Due to the difference in corrosion potential, galvanic corrosion of α_{Al} matrix in the contact with cathodic phase occurs and propagates through the matrix, as peripheral matrix dissolution [32]. A similar intermetallic phase, Al_2MgCu (S-phase), is present left from Al_2Cu intermetallic phase. This phase is anodic in nature with respect to the matrix. Further proof of the anodic properties of this phase is that no sign of corrosion was observed in the case of this alloy after PD test. Namely, for this phase, a high breakdown potential is reported [15, 33]. At higher potential and current densities, which were not reached during the PD polarization within this study, S-phase is dealloyed, accompanied by Cu enrichment in near vicinity [29].

Corrosion attack in QC alloy after PD test is presented in Fig. 8. Here, similarly to the previously presented alloy, the dissolution of the α_{Al} matrix took place. At several sites, "islands" of self-standing Al-Mn quasicrystals are surrounded by corroded α_{Al} (see black arrow in Fig. 8a). On the other hand, Al_2Cu (θ) intermetallic phase presence was not observed to cause localized corrosion in the vicinity of α_{Al} as in AlSi9Cu3 alloy. For the QC alloy, the main reason for this effect is the potential difference between the matrix and the iQC phase, which is expected to be higher than that

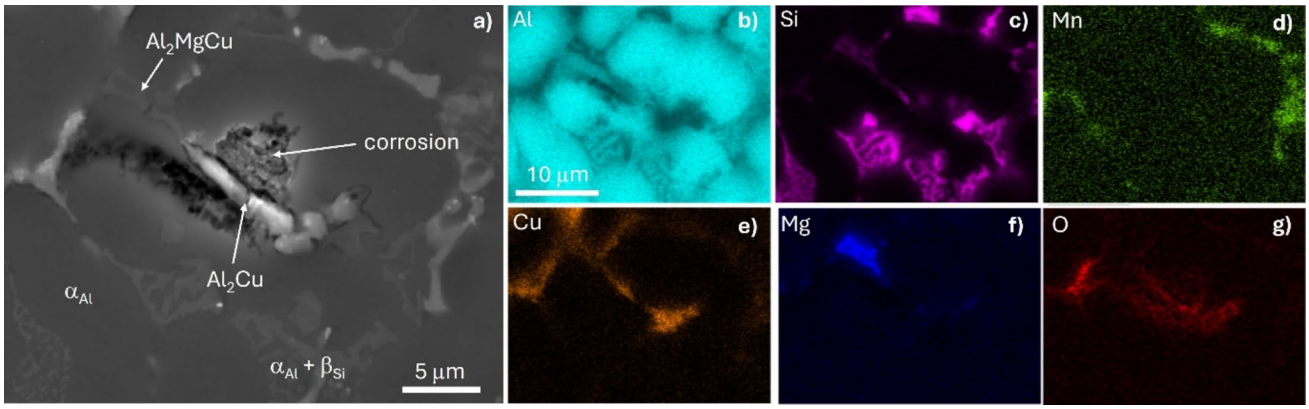

Figure 7 Backscattered SEM image (**a**) and EDS elemental mapping of the AlSi9Cu3 surface after PD polarization (**b**–**g**)

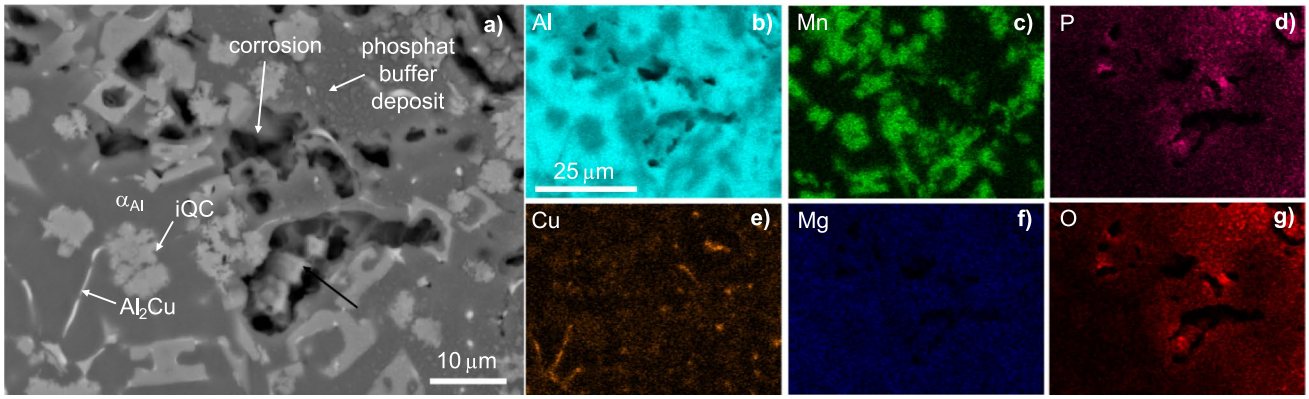

Figure 8 Backscattered SEM image (**a**) and EDS elemental mapping of the QC alloy specimens' corroded surface after PD polarization (**b**–**g**)

between the matrix and Al_2Cu. The greater potential difference in the first galvanic couple promotes matrix corrosion around the iQC phase. This suggests that, when comparing the local potentials of the iQC phase and Al_2Cu, the iQC phase should be more cathodic than Al_2Cu. Moreover, from the observed location of corrosion damage, it might be assumed that the most susceptible sites of corrosion are those with a higher density of quasicrystals over the surface. For example, α_{Al} within quasicrystals seem preferentially corroded compared to more open microstructure. Additionally, the size ratio between the cathode (iQC phase, Al_2Cu) and the anode (matrix), as well as the geometry of the phases, likely plays a role in the corrosion process. However, these relationships are complex and difficult to analyze in detail without further tests specifically focused on them.

The corrosion resistance of aluminum alloys reinforced by quasicrystals was only barely studied according to studied literature. Available studies are limited to investigation of Al-Cu-Fe and Al-Cr-Fe quasicrystals [34–37]; however, their common conclusion is that quasicrystalline phases are more resistant to corrosion, and that the selective corrosion of aluminum matrix occurs in their presence. In addition, study of Y. Massiani et al. [38] showed higher importance of elemental composition than the quasicrystalline structure. Only for two intermetallic phases containing Mn in aluminum alloys, corrosion potential are reported: for Al_6Mn which is classified as cathodic phase [14], and for $Al_{12}Mn_3Si$, for which it is assumed not to have discernible influence on corrosion of α_{Al} matrix [15]. In the case of the studied QC alloy, presented in this paper, quasicrystals are a third class of phases between crystalline and amorphous ones and are in our case composed of Al, Mn, Cu and Si. They are sharp-edged crystals

with cathodic properties regarding the bulk, around which preferential dissolution of α_{Al} matrix occurs.

Mechanical properties after environmental exposure

Results of tensile tests, performed on tensile test specimens before and after cycling in different environmental chambers (salt spray and humid chambers), are presented in Table 3. Mechanical tests conducted under laboratory conditions indicate that the QC alloy exhibits a significantly higher yield strength ($R_{p0.2}$) of approximately 276 MPa compared to AlSi9Cu3, which has a yield strength of about 193 MPa. The tensile strength (R_m) of both alloys was comparable, around 270 MPa. However, the elongation (A_{35mm}) of AlSi9Cu3 (~ 1.3%) was notably higher than that of the QC alloy (~ 0.2%). The presence of quasicrystals (iQC phase) within the Al matrix of QC alloys enhances strength and hardness [39], but on the other hand simultaneously contributes to embrittlement [40]. From these results, it can be seen that cycling in an environment containing sodium chloride reduced mechanical properties (tensile strength, R_m) of AlSi9Cu3 alloy for approximately 11% in comparison with reference specimens that were not exposed to this environment. In the case of QC alloy, the R_m was reduced by 8% in comparison with reference specimens. Cycling in a humid environment did not affect the R_m of both tested alloys in comparison with those specimens which were not exposed. From the results of mechanical tests after simulating environmental aging, one can conclude that chlorides and the temperature are a detrimental factor in the reduction of mechanical properties due to reduced corrosion resistance properties of aluminum alloys.

The primary reason for the change in tensile strength before and after cycling in a chloride-containing atmosphere is the localized dissolution around the Al_2Cu phase in the AlSi9Cu3 alloy and the corrosion of the α_{Al} matrix around the iQC phase in the QC alloy, as discussed in Sect. "Surface investigation after potentiodynamic polarization". This localized corrosion creates a notching effect, reducing the maximum force in the tensile test, leading to earlier rupture and consequently resulting in an apparent reduction in fracture elongation.

Conclusion

This study compared the corrosion behavior of a novel high-pressure die-cast quasicrystalline aluminum alloy with that of the conventional AlSi9Cu3 alloy in a near-neutral phosphate buffer solution with low chloride content. The two alloys exhibit significant differences in chemical composition, leading to distinct microstructural characteristics. The microstructure of AlSi9Cu3 alloy consists primarily of an α_{Al}-matrix and Si, along with intermetallic phases such as Al_2Cu, Al_2CuMg and minor amounts of Fe- and Mn-rich phases. In contrast, the QC alloy is dominated by an icosahedral quasicrystalline (iQC) phase, with smaller amounts of intermetallic phases, including the quasicrystalline approximant β-AlFeSi.

Corrosion characterization indicates that the QC alloy exhibits comparable, and in some cases improved, corrosion resistance compared to AlSi9Cu3.

In AlSi9Cu3 alloy, the cathodic Al_2Cu phase accelerates preferential dissolution of the α_{Al}-matrix due to electrochemical potential differences.

Although Al_2Cu is also present in the QC alloy, the primary galvanic interaction occurs between the iQC phase and the α_{Al}-matrix, thus leading to localized α_{Al}-matrix dissolution.

Table 3 Results of tensile tests on AlSi9Cu3 and QC alloy before the exposure, and after 10 cycles of exposure in salt, or humid chamber

	Type of environmental exposure	$Rp_{0.2}$ [MPa]	R_m [MPa]	A_{35mm} [%]
AlSi9Cu3	Reference	193 ± 1	272 ± 7	1.3 ± 0.2
	Salt spray chamber	189 ± 2	240 ± 15	0.9 ± 0.2
	Humid chamber	193 ± 2	271 ± 11	1.5 ± 0.2
QC alloy	Reference	276 ± 0.0*	270 ± 16	0.2 ± 0.1
	Salt spray chamber	n/d	249 ± 12	0.1 ± 0.0
	Humid chamber	279 ± 6	291 ± 0.5	0.3 ± 0.0

*determined only on one specimen of 3

These findings suggest that the incorporation of quasicrystalline phases in aluminum alloys may offer potential benefits in mitigating corrosion while enhancing mechanical properties.

Acknowledgements

The research work was implemented in the frame of CastQC—A novel cast ultra-high-specific strength quasicrystal aluminum alloy (No. 21128), project co-funded by the EU through the EIT RawMaterials funding scheme in the frame of Horizon Europe, and co-financed by the Slovenian Research Agency through the core research program P2-0273.

Author contribution

M. Bajt Leban was involved in conceptualization, writing (original draft, review & editing), investigation, methodology, formal analysis, funding acquisition; T. Drevenšek helped in formal analysis, writing (original draft); T. Kosec contributed to writing (original draft), methodology, formal analysis, funding acquisition, supervision; B. Leskovar was involved in formal analysis, writing (original draft); B. Markoli helped in formal analysis, writing (original draft).

Funding

HORIZON EUROPE Framework Programme, 21128, Mirjam Bajt Leban, Javna Agencija za Raziskovalno Dejavnost RS, P2-0273, Tadeja Kosec.

Declarations

Conflict of interest The authors declare that they have no known competing financial interests or personal relationships that could have appeared to influence the work reported in this paper.

Supplementary Information The online version contains supplementary material available at https://doi.org/10.1007/s10853-025-11046-7.

References

[1] Li S, Yue X, Li Q et al (2023) Development and applications of aluminum alloys for aerospace industry. J Mater Res Technol 27:944–983. https://doi.org/10.1016/j.jmrt.2023.09.274

[2] Aglawe K, Giri S, Dhande M, Shelare S (2023) Application of aluminum alloys in aviation industry: a review. AIP Conf Proc 2800:020064. https://doi.org/10.1063/5.0163002

[3] Miller WS, Zhuang L, Bottema J et al (2000) Recent development in aluminium alloys for the automotive industry. Mater Sci Eng, A 280:37–49. https://doi.org/10.1016/S0921-5093(99)00653-X

[4] Benedyk JC (2010) 3 - Aluminum alloys for lightweight automotive structures. In: Mallick PK (ed) Materials, Design and Manufacturing for Lightweight Vehicles. Woodhead Publishing, pp 79–113

[5] You X, Xing Z, Jiang S et al (2024) A review of research on aluminum alloy materials in structural engineering. Dev Built Environ 17:100319. https://doi.org/10.1016/j.dibe.2023.100319

[6] Georgantzia E, Gkantou M, Kamaris GS (2021) Aluminium alloys as structural material: a review of research. Eng Struct 227:111372. https://doi.org/10.1016/j.engstruct.2020.111372

[7] Kores S, Strmšek S, Vončina M, Medved J (2023) Innovative approaches in development of aluminium alloys for packaging industry. In: Broek S (ed) Light Metals 2023. Springer Nature Switzerland, Cham, pp 535–541

[8] Davis JR, ASM International (2007) Aluminum and aluminum alloys. ASM International, Materials Park, Ohio, pp 351–416

[9] Shechtman D, Blech I, Gratias D, Cahn JW (1984) Metallic phase with long-range orientational order and no translational symmetry. Phys Rev Lett 53:1951–1953. https://doi.org/10.1103/PhysRevLett.53.1951

[10] Naglič I, Samardžija Z, Delijić K et al (2017) Metastable quasicrystals in Al–Mn alloys containing copper, magnesium and silicon. J Mater Sci 52:13657–13668. https://doi.org/10.1007/s10853-017-1477-8

[11] Dubois J-M (2005) Useful quasicrystals. World Scientific, Hackensack

[12] The European Green Deal - European Commission (2021) https://commission.europa.eu/strategy-and-policy/priorities-2019-2024/european-green-deal_en. Accessed 18 Oct 2024

[13] Vargel C (2020) Corrosion of aluminium, 2nd edn. Elsevier, Cambridge

[14] Tao J (2016) Surface composition and corrosion behavior of an Al-Cu alloy. In: HAL open science. https://api.semanticscholar.org/CorpusID:136298108. Accessed 15 Jan 2025

[15] Birbilis N, Buchheit RG (2005) Electrochemical characteristics of intermetallic phases in aluminum alloys. J Electrochem Soc 152:B140–B151. https://doi.org/10.1149/1.1869984

[16] Monticelli C, Zanotto F, Balbo A et al (2022) Corrosion behavior of high-pressure die-cast secondary AlSi9Cu3(Fe) alloy. Corros Sci 209:110779. https://doi.org/10.1016/j.corsci.2022.110779

[17] Leard RR, Buchheit RG (2002) Electrochemical characterization of copper-bearing intermetallic compounds and localized corrosion of Al-Cu-Mg-Mn Alloy 2024. MSF 396–402:1491–1496. https://doi.org/10.4028/www.scientific.net/MSF.396-402.1491

[18] Davoodi A, Pan J, Leygraf C, Norgren S (2008) Multi-analytical and In situ studies of localized corrosion of EN AW-3003 alloy—influence of intermetallic particles. J Electrochem Soc 155:C138–C146. https://doi.org/10.1149/1.2834454

[19] Zamin M (1981) The role of Mn in the corrosion behavior of Al-Mn alloys. Corrosion 37:627–632. https://doi.org/10.5006/1.3577549

[20] Moffat TP, Stafford GR, Hall DE (1993) Pitting corrosion of electrodeposited aluminum-manganese alloys. J Electrochem Soc 140:2779–2786. https://doi.org/10.1149/1.2220910

[21] Naglič I, Samardžija Z, Delijić K et al (2018) Synthesis of an Al–Mn-based alloy containing in situ-formed quasicrystals and evaluation of its mechanical and corrosion properties. JOM 70:2698–2703. https://doi.org/10.1007/s11837-018-2945-6

[22] Zupanic F, Boncina T, Rozman N et al (2008) Development of an Al–Mn–Be–Cu alloy with improved quasicrystalline forming ability. Z Kristallogr 223:735–738. https://doi.org/10.1524/zkri.2008.1037

[23] Zupanič F, Wang D, Gspan C, Bončina T (2015) Precipitates in a quasicrystal-strengthened Al–Mn–Be–Cu alloy. Mater Charact 106:93–99. https://doi.org/10.1016/j.matchar.2015.05.013

[24] Zhang X, Wang D, Zhou Y et al (2021) Exploring crystal structures, stability and mechanical properties of Fe, Mn-containing intermetallics in Al-Si Alloy by experiments and first-principles calculations. J Alloy Compd 876:160022. https://doi.org/10.1016/j.jallcom.2021.160022

[25] Leskovar B, Šturm S, Samardžija Z et al (2018) Epitaxial growth of a metastable icosahedral quasicrystal on a stable icosahedral quasicrystal substrate. Scripta Mater 150:92–95. https://doi.org/10.1016/j.scriptamat.2018.03.014

[26] Zhang Z, Sun X, Huang S et al (2021) Microstructure, mechanical properties and corrosion behavior of the aluminum alloy components repaired by cold spray with Al-based powders. Metals 11:1633. https://doi.org/10.3390/met11101633

[27] Kakinuma H, Muto I, Oya Y et al (2021) Morphological change and open-circuit potential of single metastable pit on AA1050 aluminum in NaCl solution. J Electrochem Soc 168:021504. https://doi.org/10.1149/1945-7111/abdee9

[28] Marcus P, Mansfeld FB (2005) Analytical methods in corrosion science and engineering, 1st edn. CRC Press, Boca Raton, pp 502–517

[29] Mazurkiewicz B, Piotrowski A (1983) The electrochemical behaviour of the Al_2Cu intermetallic compound. Corros Sci 23:697–707. https://doi.org/10.1016/0010-938X(83)90034-3

[30] Charalampidou C, Dietzel W, Zheludkevich M et al (2021) Corrosion-induced mechanical properties degradation of Al-Cu-Li (2198–T351) aluminium alloy and the role of side-surface cracks. Corros Sci 183:10933. https://doi.org/10.1016/j.corsci.2021.109330

[31] Zhou H (2017) Corrosion behavior of the Al2Cu intermetallic compound and coupled Al2Cu/Al. Int J Electrochem Sci 12:9542–9554. https://doi.org/10.20964/2017.10.32

[32] Büchler M, Watari T, Smyrl WH (2000) Investigation of the initiation of localized corrosion on aluminum alloys by using fluorescence microscopy. Corros Sci 42:1661–1668. https://doi.org/10.1016/S0010-938X(00)00020-2

[33] Buchheit RG, Montes LP, Martinez MA et al (1999) The electrochemical characteristics of bulk-synthesized Al2CuMg. J Electrochem Soc 146:4424–4428. https://doi.org/10.1149/1.1392654

[34] Rüdiger A, Köster U (2000) Corrosion behavior of Al-Cu-Fe quasicrystals. Mater Sci Eng, A 294:890–893. https://doi.org/10.1016/S0921-5093(00)01037-6

[35] Babilas R, Bajorek A, Spilka M et al (2020) Structure and corrosion resistance of Al–Cu–Fe alloys. Progress Nat Sci: Mater Int 30:393–401. https://doi.org/10.1016/j.pnsc.2020.06.002

[36] Lee K, Chen E, Naugle D, Liang H (2021) Corrosive behavior of multi-phased quasicrystal alloys. J Alloy Compd 851:156862. https://doi.org/10.1016/j.jallcom.2020.156862

[37] Pashangeh S, Alizadeh M, Amini R (2022) Structural and corrosion behavior investigation of novel nano-quasicrystalline Al-Cr-Fe reinforced Al-matrix composites produced by ARB process. J Alloy Compd 890:161774. https://doi.org/10.1016/j.jallcom.2021.161774

[38] Massiani Y, Ait Yaazza S, Crousier JP, Dubois JM (1993) Electrochemical behaviour of quasicrystalline alloys in corrosive solutions. J Non-Cryst Solids 159:92–100. https://doi.org/10.1016/0022-3093(93)91286-C

[39] Coury FG, Kiminami CS, Botta WJ et al (2016) Design and production of Al-Mn-Ce alloys with tailored properties. Mater Des 110:436–448. https://doi.org/10.1016/j.matdes.2016.08.008

[40] Schurack F, Eckert J, Schultz L (2001) Synthesis and mechanical properties of cast quasicrystal-reinforced Al-alloys. Acta Mater 49:1351–1361. https://doi.org/10.1016/S1359-6454(01)00045-3